Microwave Circuit Models of Semiconductor Injection Lasers

RODNEY S. TUCKER AND DAVID J. POPE

Abstract—**Small-signal two-port circuit models of packaged commerical broad-stripe and buried-heterojunction AlGaAs laser diodes are presented. The models are based on the single-mode rate equations, and include the heterojunction $I-V$ and space-charge characteristics. Also included are package and substrate parasitics. The models agree well with measured reflection coefficient and modulation frequency response data, and can be incorporated in standard microwave circuit analysis programs.**

I. Introduction

THE SEMICONDUCTOR injection laser is well established as an important light source for fiber-optical and integrated-optical systems [1]. Recently, it has also found application in optically controlled microwave circuits such as switches [2] and injection-locked oscillators [3].

In the analysis and design of optical and microwave circuits using directly modulated laser diodes, it is often necessary to determine the dynamic response of the laser for a given electrical input signal. This response is influenced by a number of factors. For example, electrooptical resonances [1], [4] give rise to peaks in the small-signal frequency response and electrical effects such as package parasitics [5], and space-charge capacitance [6], [7] also modify the response.

Traditionally, the modulation response of the laser has been determined using a direct solution of the rate equations [1], [4]. This method of analysis has several disadvantages: it requires specialized software, it is not suited to the inclusion of package parasitics, and device-circuit interactions are not easily taken into account. An alternative approach is to use a circuit analysis based on a circuit model of the device. However, to date very little has been published on circuit models for laser diodes.

This paper presents examples of laser diode small-signal circuit models that can be easily incorporated in conventional microwave circuit analysis programs. Element values are given for commercial diodes from two different laser manufacturers. The models include the effects of package parasitics, space-charge capacitance, heterojunction $I-V$ characteristics, and electrooptical dynamics in the active layer. Thus, the major factors which contribute to the small-signal dynamic response of the laser are taken into account. In all previous reports of laser diode circuit models ([5], [7], [8], for example) at least one of these effects has been neglected.

Manuscript received July 13, 1982; revised September 9, 1982. This work was supported by the Australian Research Grants Committee and Telecom Australia. Part of this work was presented at the 1982 IEEE MTT-S International Microwave Symposium, Dallas, Texas, June 15-17, 1982.

R. S. Tucker was with the Department of Electrical Engineering, University of Queensland, St. Lucia, Queensland 4067, Australia. He is now with Bell Laboratories, Crawford Hill Laboratory, Holmdel, NJ 07733, on leave from the University of Queensland.

D. J. Pope is with the Department of Electrical Engineering, University of Queensland, St. Lucia, Queensland 4067, Australia.

II. Small-Signal Circuit Models

The key to the models presented here is a small-signal circuit model of the intrinsic device chip. This basic model is cascaded with a model of the package to give a two-port circuit model of the complete laser. The input port of the model corresponds to the electrical terminals of the packaged device, and the voltage at the output port is an analog of the light output intensity. The chip model is described in this Section, and in Section III the complete model is illustrated for two commercial lasers.

A. The Rate Equations

The chip model is based on the well-known single-mode rate equations [4], [9], with a space-charge capacitance term added. Neglecting lateral diffusion [1], the rate equations can be written in the following form:

$$\frac{dN}{dt} + \frac{C_{sc}}{\alpha} \cdot \frac{dV_j}{dt} = \frac{I_j}{\alpha} - \frac{N}{\tau_n} - GS \tag{1}$$

$$\frac{dS}{dt} = GS - \frac{S}{\tau_p} + \beta \frac{N}{\tau_n} \tag{2}$$

where N is the active layer excess electron density, S is the photon density, τ_n and τ_p are the electron and photon lifetimes, I_j and V_j are the current and voltage at the diode junction, C_{sc} is the space-charge capacitance, G is the optical gain in the active layer, β is the spontaneous emission coefficient, and $\alpha = qv_a$ where q is electronic charge and v_a is the volume of the active layer. The optical gain is given by [4]

$$G = \gamma(N - N_g) \tag{3}$$

where γ and N_g are constants.

The device parameters α, β, γ, and τ_p depend on the geometry of the active layer and other physical properties of the chip [1]. Since it is difficult to determine the active layer dimensions accurately, the geometrical details are not used explicitly and the chip is modeled in terms of the parameters in (1)–(3). For simplicity, carrier diffusion is

0018-9480/83/0300-0289$01.00 ©1983 IEEE

not included in the model. However, the device parameters can be considered as *effective* parameters whose values are adjusted to provide some allowance for diffusion and other effects not included in (1) and (2).

An important step in the present analysis is to relate the electron density in (1) and (2) to the diode junction voltage. This is achieved by approximating the heterojunction $N-V_j$ characteristic with a classical Shockley relationship

$$N = N_e\left[\exp(qV_j/\eta kT)-1\right] \tag{4}$$

where N_e is the equilibrium electron density and $\eta \simeq 2$ for AlGaAs devices [6].

To obtain the small-signal circuit model of the chip it is necessary first to linearize (1)–(4). This is carried out using the following notation. Steady-state or dc components of I_j, N, S, and G are written as I_0, N_0, S_0, and G_0, respectively, and the small-signal ac (incremental) components are assumed to have sinusoidal waveforms and are expressed in phasor form using lower case symbols. Thus, $N = N_0 + ne^{j\omega t}$ and $S = S_0 + se^{j\omega t}$ where ω is the radian frequency and $j = \sqrt{-1}$.

Using this notation, and with (4) substituted, (1) and (2) are easily linearized. Since the incremental terms are small, products of incremental terms are very small and can be neglected. Thus, the rate equations reduce to

$$i_j = v_j(1/R_1 + j\omega C_t) + \alpha G_0 s \tag{5}$$

and

$$\alpha s(G_3 + j\omega) = v_j G_2 \tag{6}$$

where

$$R_1 = \left(R_d^{-1} + R_4^{-1}\right)^{-1}$$

$$G_2 = \left(\beta/R_d + R_4^{-1}\right)$$

$$G_3 = \frac{\alpha\beta G_0 N_0}{\tau_n I_0 - N_0\alpha}$$

and

$$R_4 = R_d G_3(\beta N_0 \gamma)^{-1}.$$

The small-signal diode junction resistance is $R_d = 2\tau_n kT/q\alpha N_0$ and the total diode capacitance is $C_t = C_d + C_{sc}$ where $C_d = \tau_n/R_d$ is the active layer diffusion capacitance.

The junction resistance, diffusion capacitance, R_1, G_2, G_3, and R_4 are all easily evaluated in terms of the dc component N_0 of electron density. This electron density is, in turn, obtained from the dc drive current I_0 using (1) and (2) with the derivatives set to zero. This gives a quadratic in N_0

$$N_0^2(1-\beta) - N_0\left[\frac{1}{\gamma\tau_p} + \frac{\tau_n I_0}{\alpha} + (1-\beta)N_g\right] + \left[\frac{1}{\gamma\tau_p} + N_g\right]\frac{\tau_n I_0}{\alpha} = 0. \tag{7}$$

It can be shown that the correct value of N_0 is the smaller of the two solutions to (7). The threshold current I_{th} is given by [4]

$$I_{\text{th}} = \alpha(1-\beta)\left(\frac{1}{\tau_p\gamma} + N_g\right)/\tau_n. \tag{8}$$

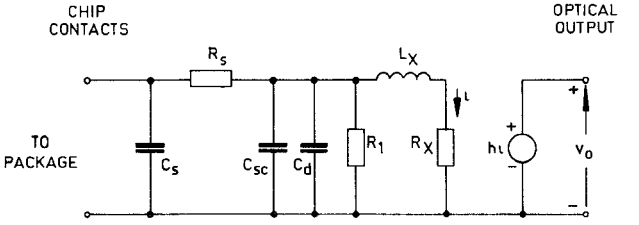

Fig. 1. Circuit model of the laser chip, including series resistance R_s and parasitic capacitance C_s.

B. Chip Circuit Model

The input (electrical) section of the small-signal chip model is obtained here from the small-signal input admittance Y_d at the heterojunction. From (5) and (6) it can be shown that this admittance is

$$Y_d = i_j/v_j = \frac{1}{R_1} + j\omega C_t + \frac{1}{R_x + j\omega L_x} \tag{9}$$

where $L_x = (G_0G_2)^{-1}$ and $R_x = G_3L_x$. The admittance Y_d can be modeled as a shunt RC circuit in shunt with a series RL circuit, and forms the basis of the small-signal laser chip model as shown in Fig. 1. Also included in the model is a series resistance R_s which accounts for contact resistance and bulk resistance in the semiconductor chip, and a capacitance C_s which represents parasitic capacitance associated with the chip.

For a dc bias current I_0 below threshold, the effects of stimulated emission can be ignored. Under these conditions the resistances R_4 and R_x are large and the model reduces to a simple forward-biased diode with small-signal resistance R_d and shunt capacitance C_t. This model has been used by previous authors [5], [6], [7]. Above threshold, stimulated emission strongly influences the electrical characteristics of the device, and R_4 and R_x cannot be neglected.

The optical output port of the model is also obtained from (5) and (6). It can be shown from these equations that the small-signal photon density s is proportional to the small-signal current i shown in Fig. 1. The current-controlled voltage source in Fig. 1 thus provides a voltage v_o at the output port of the model which is an analog of the small-signal photon density in the laser. The output voltage of the model can therefore be used as a measure of the small-signal light output intensity from the laser. The transimpedance of the current-controlled voltage source is independent of frequency. It is given by

$$h = (\alpha G_0)^{-1}. \tag{10}$$

In frequency response calculations, the magnitude of v_o is usually determined relative to its value at zero frequency. The absolute value of v_o is therefore not required, and the transimpedance h can be scaled by any convenient factor that gives reasonable numerical values for v_o.

C. Packages

Commercial laser diodes are available in a wide variety of packages. The packages for the two devices considered here are illustrated in Fig. 2. The first device, a broad-stripe double heterojunction laser (Laser Diode Labs LCW-10)

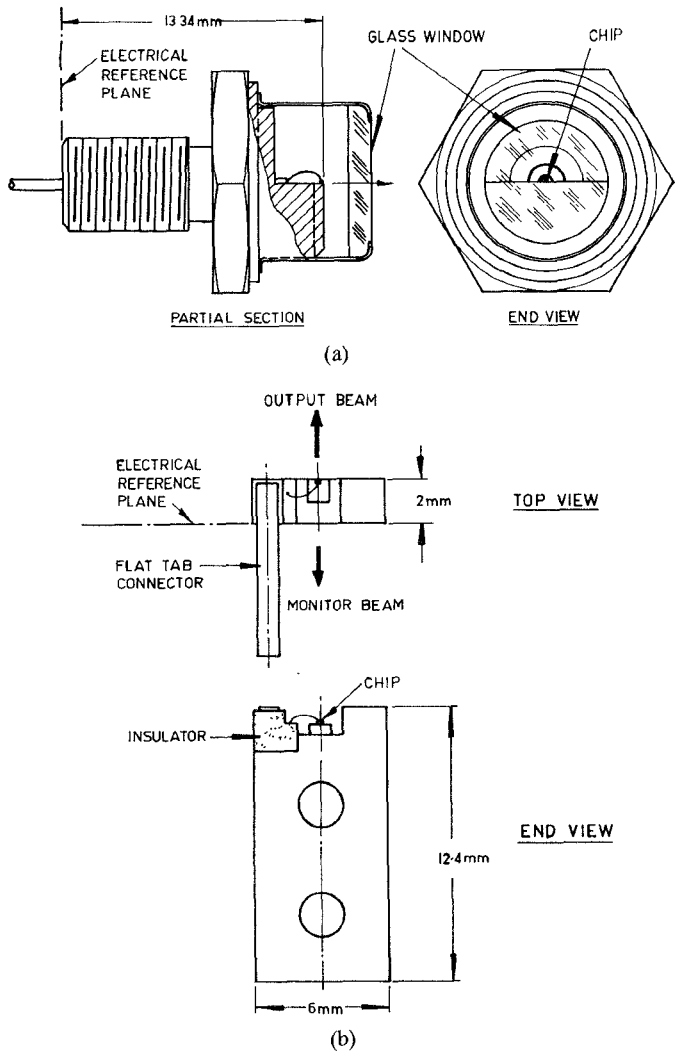

Fig. 2. Package outlines for (a) the broad-stripe laser and (b) the BH laser. Electrical reference planes used in the reflection coefficient measurements are shown.

has a package that provides good protection of the chip from possible mechanical damage, but has relatively large electrical parasitics. For the second device, a buried heterostructure (BH) laser (Hitachi HLP-3400), the chip is mechanically unprotected, but the parasitics are much smaller. Circuit models for these packages are given in the next section.

III. Device Characterization and Modeling

The small-signal laser model is illustrated here with numerical examples for the two commerical lasers. Parameter values for the models were obtained from measured reflection coefficient and frequency response characteristics.

A. Measurements

The experimental arrangement used to characterize the lasers is shown in Fig. 3. The devices were mounted in 50-Ω microstrip test fixtures. These test fixtures were temperature-stabilized with a Peltier element to within $\pm 0.2°C$ at room temperature. This minimized drift of the threshold current and consequent changes in the modulation response characteristics [1]. Broad-band electrical reflection

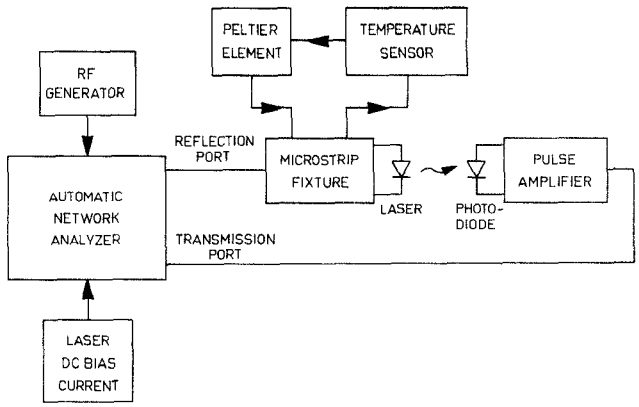

Fig. 3. Experimental arrangement for reflection coefficient measurements and frequency response measurements.

coefficient data referred to the device terminals were obtained using an automatic network analyzer. The modulation frequency response was also measured using the network analyzer. For this measurement, the lasers were driven from the 50-Ω internal resistance of the network analyzer reflection port, and the light output was detected with a high-speed photodetector (Opto-electronics PD10-01) and a broad-band (2 kHz–5.5 GHz) pulse amplifier (B&H AC5120).

Care was taken to ensure that the laser was loosely coupled to the photodetector. Loose coupling ensures that the amount of light reflected back into the laser is minimized, while providing sufficient detected signal power for reliable frequency response measurements. Using a number of different coupling arrangements, it was shown that light reflected back into the laser did not significantly affect the frequency response [10] or introduce undue noise [11] into the system. The frequency response of the photodetector and pulse amplifier was estimated from time domain measurements using a pulsed laser with known pulse shape (determined using a streak camera). This information was used to correct for the finite bandwidth of the detection system.

B. Model Parameters

Parameters of the small-signal models for each device were obtained by computer-aided fitting of the modeled reflection and transmission characteristics to the measured data. Details of this procedure are as follows.

i) The devices were forward-biased above threshold. Under these conditions, the resistance R_1 is small and the input impedance at the heterojunction is approximately zero. Based on their physical layout, models of the packages were proposed and the element values of these packages, along with the substrate resistance and capacitance (R_s and C_s), were obtained by fitting the modeled input reflection coefficient to the measured data.

ii) The above procedure was repeated with zero bias. Under these conditions, R_1 and R_x (Fig. 1) approach infinity, and C_d is zero. With the package and substrate parasitics known from i) above, the zero-bias space-charge capacitance $C_{sc(0)}$ was obtained from the measured reflection coefficient data. The forward-bias value of space-

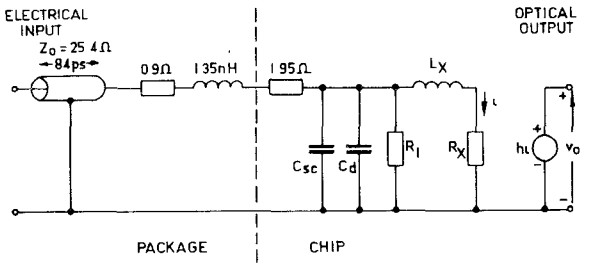

Fig. 4. Circuit model of the broad-stripe laser.

TABLE I
DEVICE PARAMETERS FOR THE LCW-10

Parameter	Unit	Value
τ_n	ns	3.95
τ_p	ps	1.28
α	Am^3s	2.30×10^{-34}
β		1.86×10^{-4}
γ	$s^{-1}m^3$	9.21×10^{-13}
N_g	m^{-3}	1.07×10^{24}
I_{th}	mA	112

TABLE II
CIRCUIT ELEMENT VALUES FOR THE LCW-10 MODEL

I_0(mA)	C_{sc}(pF)	C_d(nF)	$R_1(\Omega)$	L_x(pH)	$R_x(m\Omega)$
117	138	8.59	0.416	5.62	17.6
121	138	8.60	0.388	3.20	5.70
125	138	8.60	0.363	2.23	2.77

charge capacitance was obtained using the relationship [6]

$$C_{sc} = C_{sc(0)}\left(1 - V_j/V_D\right)^{-1/2} \tag{11}$$

where $V_D = 1.65$ V is the heterojunction built-in potential.

iii) The intrinsic laser parameters (τ_n, τ_p, α, β, γ, and N_g) were initially estimated using published data [1], [4]. The values of these parameters were then adjusted so that the modeled frequency response matched the measured data for a range of bias currents above threshold. In carrying out this fitting process, the parameters were constrained so that the modeled threshold current given by (8) coincided with the measured value.

IV. RESULTS

A. Broad-Stripe Laser

Fig. 4 shows the complete model for the LCW-10. The package was modeled with a length of transmission line (characteristic impedance and one-way propagation time shown), a small loss resistance, and a bondwire inductance. Table I gives values of the intrinsic device parameters and Table II gives element values of the chip model for three values of dc bias current I_0 (117, 121, and 125 mA). The threshold current of the device was 112 mA. The forward-bias space-charge capacitance C_{sc} was found to be 138 pF. It is felt that this is more realistic than the very large values for C_{sc} used by Dumant *et al.* [7] for a similar device.

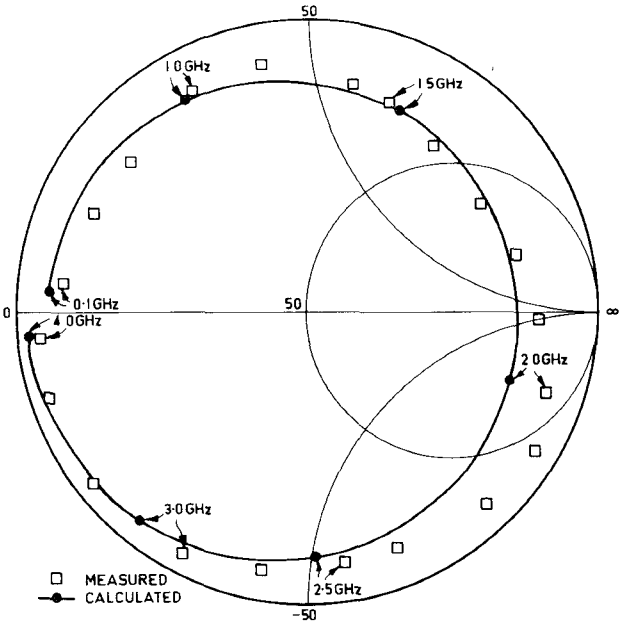

Fig. 5. Measured and calculated reflection coefficient of the broad-stripe laser biased above threshold.

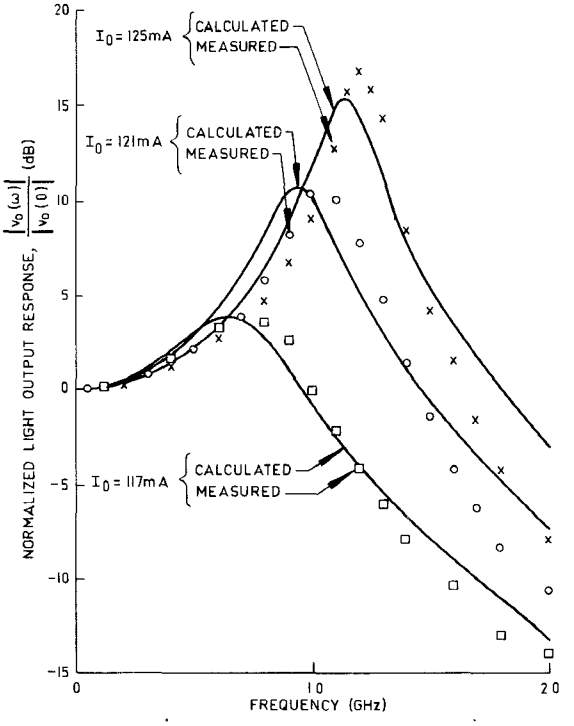

Fig. 6. Measured and calculated small-signal frequency response of the broad-stripe laser for three different values of bias current above threshold.

Fig. 5 shows the measured and calculated reflection coefficient for the LCW-10, forward-biased at a current of $I_0 = 121$ mA. The measured and calculated modulation frequency response[1] is given in Fig. 6 at three bias currents

[1]The results given here are based on an improved estimate of the photodetector bandwidth which is more accurate than was used in [12].

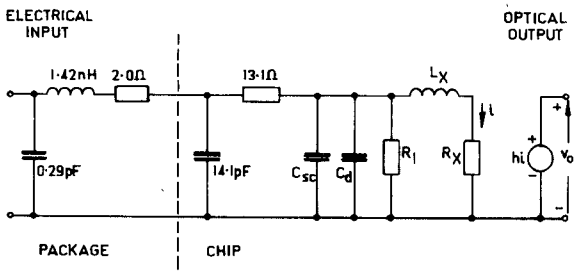

Fig. 7. Circuit model of the BH laser.

TABLE III
DEVICE PARAMETERS FOR THE HLP-3400

Parameter	Unit	Value
τ_n	ns	1.12
τ_p	ps	6.0
α	Am^3s	4.60×10^{-36}
β		8.70×10^{-3}
γ	$s^{-1}m^3$	2.60×10^{-13}
N_g	m^{-3}	2.57×10^{24}
I_{th}	mA	13

TABLE IV
CIRCUIT ELEMENT VALUES FOR THE HLP-3400 MODEL

I_0(mA)	C_{sc}(pF)	C_d(pF)	R_1(Ω)	L_x(pH)	R_x(mΩ)
20	10.0	286	1.07	8.90	24.0
30	10.0	287	0.524	3.65	4.07

for frequencies up to 2 GHz. The frequency response shows the well-known effects of electrooptical resonance [1]. Agreement between the experimental and theoretical data is good. The modeling procedure was repeated for a second LCW-10 with a different threshold current. The package model remained the same, but the parameters α, τ_p, and N_g showed a significant variation between devices.

B. Buried-Heterostructure Laser

The circuit model of the HLP-3400 is shown in Fig. 7. Table III gives the device parameters for the HLP-3400, and Table IV gives element values of the chip model at two values of bias current above threshold. The threshold current of the device was 13 mA. The package model of the HLP-3400 is relatively simple. However, the parasitic capacitance and resistance (14.1 pF and 13.1 Ω, respectively) are quite large. The measured and calculated reflection coefficient and modulation frequency response[1] of the HLP-3400 are shown in Figs. 8 and 9, respectively. Agreement between the measured and calculated data is good.

As expected [1], the resonance peak in the frequency response is much smaller for the BH laser than the broad-stripe laser. This increased damping in the BH laser is

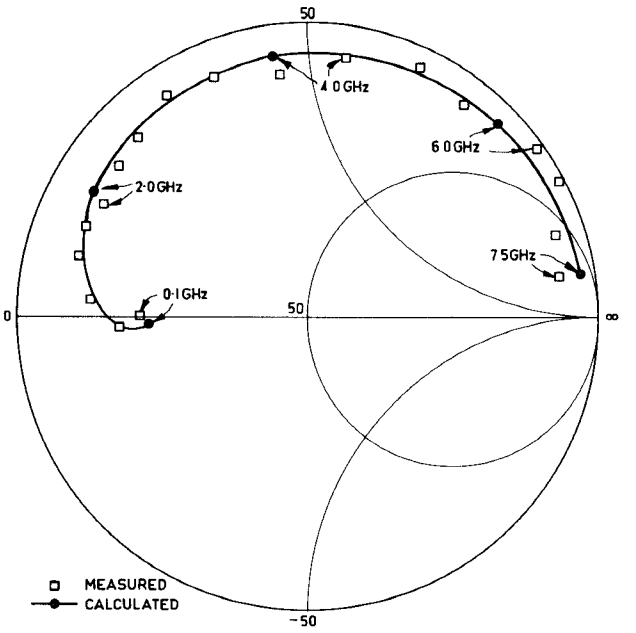

Fig. 8. Measured and calculated reflection coefficient of the BH laser biased above threshold.

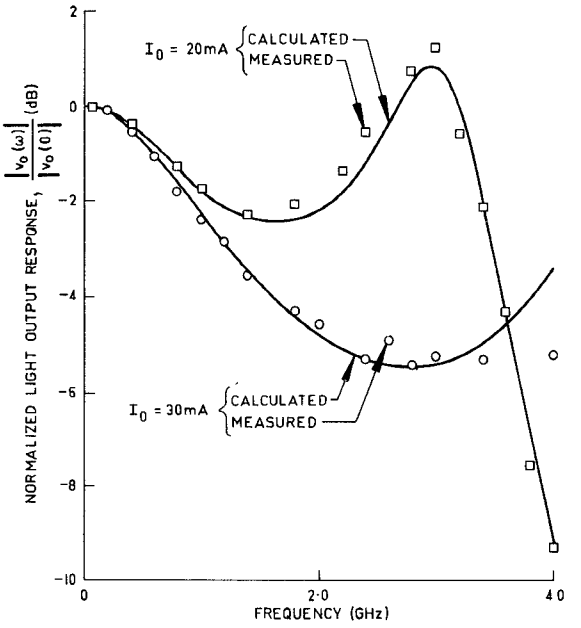

Fig. 9. Measured and calculated small-signal frequency response of the BH laser for two different values of bias current above threshold.

partially due to lateral diffusion in the active layer [1]. Although lateral diffusion is not included explicitly in the present model, it is accounted for approximately by using a relatively large value of the effective spontaneous emission coefficient [13]. An additional difference between the responses of the two lasers is the roll-off in the frequency response of the BH laser at frequencies *below* the resonance peak. This roll-off is of significance since it affects the ultimate bandwidth of the device. A study of the model in Fig. 7 has shown that the roll-off is caused mainly by the parasitic capacitance C_s and the substrate resistance R_s. For improved device bandwidth, these elements should be reduced in value.

V. Conclusion

Accurate circuit models have been presented for two commercial packaged semiconductor laser diodes. Element values for the models were obtained using measured reflection and transmission frequency response data. The models show good agreement with measurements over a wide range of frequencies and dc bias levels. They can be easily incorporated in standard microwave circuit analysis programs, and should find application in the analysis and design of optical and microwave circuits. A significant feature of the circuit models is that they enable the influence of substrate and package parasitics to be evaluated, and facilitate the inclusion of device-circuit interactions in calculated response characteristics.

Acknowledgment

The laser diodes were supplied by T. E. Stockton of Laser Diode Labs, and N. Chinone of Hitachi.

References

[1] H. Kressel, Ed., *Semiconductor Devices for Optical Communications*, Topics in Applied Physics, vol. 39, New York: Springer-Verlag, 1980.

[2] R. A. Kiehl and D. M. Drury, "Performance of optically coupled microwave switching devices," *IEEE Trans. Microwave Theory Tech.*, vol. MTT-29, pp. 1004–1010, Oct. 1981.

[3] J. R. Forrest and A. A. Salles, "Optics control microwaves," *Microwave Syst. News*, vol. 11, no. 6, pp. 112–122, June 1981.

[4] P. M. Boers, M. T. Vlaardingerbroek, and M. Danielsen, "Dynamic behaviour of semiconductor lasers," *Electron. Lett.*, vol. 11, pp. 206–208, May 15, 1975.

[5] M. Maeda, K. Nagano, M. Tanaka, and K. Chiba, "Buried-heterostructure laser packaging for wideband optical transmission systems," *IEEE Trans. Commun.*, vol. COM-26, pp. 1076–1081, July 1978.

[6] T. P. Lee, "Effect of junction capacitance on the rise-time of LED's and the turn-on delay of injection lasers," *Bell Syst. Tech. J.*, vol. 54, pp. 53–68, 1975.

[7] J. M. Dumant, Y. Guillausseau, and M. Monerie, "Small-signal modulation of DH laser diodes: Effect of the junction capacitance," *Opt. Commun.*, vol. 33, pp. 188–192, May 1980.

[8] J. Katz, S. Margalit, C. Harder, D. Wilt, and A. Yariv, "The intrinsic electrical equivalent circuit of a laser diode," *IEEE J. Quantum Electron.*, vol. QE-17, pp. 4–7, Jan. 1981.

[9] R. S. Tucker, "Large-signal circuit model for simulation of injection-laser modulation dynamics," *Proc. Inst. Elec. Eng.*, vol. 128, Part I, pp. 180–184, Oct. 1981.

[10] R. P. Salathé, "Diode lasers coupled to external resonators," *Appl. Phys.*, vol. 20, pp. 1–18, Jan. 1979.

[11] O. Hirotu *et al.*, "Properties of intensity noises of laser diodes due to reflected waves from single-mode optical fibres and its reduction," *IEEE J. Quantum Electron.*, vol. QE-17, pp. 1014–1020, June 1981.

[12] R. S. Tucker and D. J. Pope, "Microwave circuit models of semiconductor injection lasers," in *IEEE MTT-S Int. Microwave Symp. Dig.*, June 1982, pp. 104–106.

[13] R. S. Tucker and D. J. Pope, "Circuit modeling of diffusion-induced damping in semiconductor lasers," to be published in *IEEE J. Quantum Electron.*, vol. QE-19.

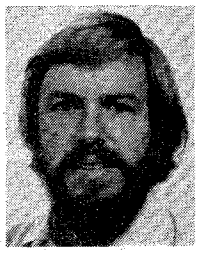

Rodney S. Tucker was born in Melbourne, Australia, in March 1948. He received the B.E. and Ph.D. degrees from the University of Melbourne, Australia, in 1969 and 1975, respectively.

From 1973 to 1975 he was a Lecturer in Electrical Engineering at the University of Melbourne. In 1975 he was awarded a Harkness Fellowship for two years' postdoctoral study in the U.S.A. During 1975–1976 he was with the Department of Electrical Engineering and Computer Sciences, University of California, Berkeley, and during 1976–1977 he was with the School of Electrical Engineering, Cornell University. From 1977 to 1978 he was with Plessey Research (Caswell) Ltd., Allen Clark Research Center, England. He is presently a Senior Lecturer in Electrical Engineering at the University of Queensland, Australia.

Dr. Tucker's major research interests are in microwave active and passive circuits, semiconductor optoelectronic devices, and optical communications systems.

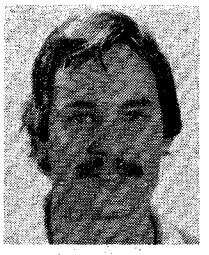

David J. Pope was born in Brisbane, Australia, on March 6th, 1959. He received the B.E. degree in electrical engineering with First Class Honours from the University of Queensland, St. Lucia, Brisbane, Australia. He is currently working towards the Ph.D. degree at the Department of Electrical Engineering, University of Queensland. His research is in the field of optoelectronic semiconductor devices.